Cellular and Molecular Biology

CMB
Cellular and Molecular Biology

Original Article

Antibacterial effect and biocompatibility of silver nanoparticle-coated bone allograft substitutes

Sanna Hadi[1*], Othman Omar[2]

Oral and maxillofacial Surgery Department, College of Dentistry, Hawler Medical University-Erbil, Erbil, Iraq

Article Info

Abstract

Osteoinduction, and/or osteoconduction, and antibacterial characteristics are prerequisites for achieving successful bone grafting. This study aimed to coat bone allografts with silver nanoparticles and assess their antibacterial activity and biocompatibility compared to uncoated bone allografts. In this study, the bone allografts were coated with varying concentrations of silver nanoparticles (5 mg/l, 10 mg/l, and 50 mg/l) through a simple adsorption technique. Subsequently, the coated samples underwent characterization using SEM, FTIR, EDS, and XRD. The Minimal Inhibitory Concentration (MIC) of the silver nanoparticles was determined against Staphylococcus aureus and Streptococcus mutans. Bacterial growth inhibition was evaluated by measuring turbidity and performing a disk diffusion test. Moreover, qualitative investigation of biofilm formation on the coated bone allograft was conducted using SEM. Following this, MG-63 cell lines, resembling osteoblasts, were cultured on the bone allografts coated with 5 mg/l of silver nanoparticles, as well as on uncoated bone allografts, to assess biocompatibility. The MIC results demonstrated that silver nanoparticles exhibited antimicrobial effects on both microorganisms, inhibiting the growth of isolates at concentrations of 0.78 mg/L for Staphylococcus aureus and 0.39 mg/L for Streptococcus mutans. The bone allografts coated with varying concentrations of silver nanoparticles exhibited significant antibacterial activity against the tested bacteria, completely eradicating bacterial growth and preventing biofilm formation. The osteoblast-like MG-63 cells thrived on the bone allografts coated with 5 mg/l of silver nanoparticles, displaying no significant differences compared to both the uncoated bone allografts and the control group. Within the limit of this study, it can be concluded that silver nanoparticles have a positive role in controlling graft infection. In addition, simple adsorption technique showed an effective method of coating without overwhelming the healing of the graft.

Keywords: Silver nanoparticles, Bone allograft, Deposition, Antibacterial activity, Biocompatibility.

1. Introduction

The success of oral rehabilitation and dental implant are mainly related to the amount and the quality of the alveolar bone. Alveolar bone loss may occur as a consequence of many issues such as, periodontal disease, periapical pathology or trauma [1]. Because the ability of bone to regenerate itself can only treat small defect sizes, bone grafting has become a crucial part of oral rehabilitation to restore a damaged ridge in a way that is both functionally and aesthetically satisfactory [2].

Different types of bone grafts are available nowadays including; autogenous bone graft, isograft, allograft, xenograft and synthetic bone substitute [3]. However, autogenous bone grafts remain the gold standard, for ideal bone grafts [4]. Despite all the advantages of using autogenous bone graft, there are major drawbacks, including; the limited availability of bone at the donor site, the extra surgery time of autogenous bone harvesting, morbidity at the donor site such as post-operative pain, hypersensitivity, paraesthesia, and infection [5].

For the reasons mentioned above, many dentists worldwide seeking an alternative bone substitute. The market for bone graft substitutes is very wide, with multiple products available, including allograft, xenograft, and artificial bone substitutes [6]. Most of the bone substitutes mentioned previously provide a good result clinically [7]. Notwithstanding the acceptable results of graft materials, each type possessed its individual shortcomings [8]. As a natural replacement for the reconstruction of bone defects, bone allografts have long been used. Since their obtainability is less limited and allows structural restoration of the skeleton. Additionally, some types of bone allograft can also provide some level of osteoinduction. For that reason, they offer an attractive alternative to bone autograft [9]. Nevertheless, allografts also come with drawbacks, notably their high cost and associated risks such as the potential for infections [8].

Overall, one of the most severe complications associated with grafting is infection, frequently resulting in adverse patient outcomes such as increased morbidity, the need for repeated surgeries, and prolonged courses of antibiotic treatment [10].

Recently, it has been reported an overall postoperative infection rate of 4.1% after bone grafting in dentistry [11].

Most of the actual bone grafts available in the market are incapable of inhibiting bacterial colonization, which can lead to infection and possible implant failure. This is attributed to the fact that the bone graft, whether temporary or permanent, behaves as a foreign entity and exhibits diminished resistance against bacterial intrusion [12]. Numerous efforts have been made to mitigate infection risks by integrating antibiotics into graft materials [13]. This involves combining certain bone substitutes with antibiotics to prevent infection or the formation of biofilms. However, antibiotic resistance leads to the use of alternative strategies to control infections, through using of metal oxides to develop antimicrobial bone graft products [13].

Metal nanoparticles, particularly silver nanoparticles, have been effectively utilized in dental applications, providing infection control and managing oral biofilms [14]. Many studies have been done to fully understand the mechanism of action of silver nanoparticles as an antimicrobial agent and preventing biofilm formation. Mathur *et al.* outlined the antibacterial mechanism of AgNPs, illustrating their ability to penetrate the cell membrane of microorganisms. This penetration increases membrane permeability, resulting in structural rupture and subsequent cell death [15]. Through the upregulation of multiple bone morphogenic proteins, AgNPs can also contribute to osteogenesis [16]. Consequently, this study hypothesizes that coating bone allografts with silver nanoparticles could have a positive impact in reducing or completely eliminating potential bacterial colonization without compromising their biocompatibility.

2. Materials and Methods
2.1. Materials
Silver nitrate ($AgNO_3$, 99.99%), and sodium borohydride ($NaBH_4$, 99.99%) were purchased from Merck, Germany. Staphylococcus aureus (ATCC: 25923) and Streptococcus mutans (ATCC: 35668) that were used in this study were from the Biotechnology Institute (Iranian Research Organization for Sciences and Technology, Tehran). MG-63 cells (ATCC: C555) were purchased from the National Centre of Genetic Resources in Iran. Demineralized freeze-dried bone allograft (DFDBA) with particle size 150-2000 μm was used as a source of bone allograft (CenoBone, Tissue Regeneration Co., Kish, Iran).

2.2. Methods
2.2.1. Silver nanoparticles synthesis
Silver nanoparticles (AgNPs) solutions were prepared using the chemical reduction method, following the same protocol as Van Dong *et al,* [17]. The procedure included adding 30 ml of 2 mM sodium borohydride ($NaBH_4$) to an Erlenmeyer flask. Magnetic stir bar was added and the flask was placed in an ice bath on a stir plate. The reason behind using an ice bath was to slow down the reaction and control the nanoparticle size and shape. After stirring and cooling the solution for 20 minutes, the solution was dripped with 2 ml of silver nitrite (0.3,0.03,0.06 mM of $AgNO_3$, for 50, 10, and 5 mg/l respectively) at approximately 1 drop per second. The stirring ceased immediately upon the complete addition of AgNO3, resulting in the solution changing to a yellowish-gray color. The color change was the result of clustering of silver ions to form monodispersed spherical nanoparticles as a transparent solution in the aqueous medium (Figure 1).

2.2.2. Bone allograft coating process
Demineralized freeze-dried bone allograft (DFDBA) with particle size 150-2000 μm (CenoBone, Tissue Regeneration Co., Kish, Iran) was coated with the chemically synthesized silver nanoparticles using simple adsorption process [18]. The synthesized silver nanoparticle solutions with different concentrations (5 mg/l, 10 mg/l and 50 mg/l) were sonicated for 4 hours (to avoid aggregation) prior to the addition of bone allograft particulate. After that, the bone allograft powders were immersed in different concentrations of AgNPs solutions for 1 hr under stirring. Then the samples were left for dryness at room temperature 27 C°.

2.3. X-ray diffraction (XRD) analysis
The crystal structure and purity of the synthesized silver nanoparticles were determined using X-ray diffraction (XRD) analysis performed with (XRD, D8, Bruker, Germany. Tests were held using a Bruker AXS D8 DISCOVER diffractometer operating at a voltage of 35 kV.

2.4. Scanning Electronic Microscopy (SEM) and Energy Dispersion X-Ray Spectroscopy (EDS):
The surface morphology of both the uncoated and silver nanoparticles (AgNPs) coated bone allografts were analysed using scanning electron microscopy (SEM, SERON TECHNOLOGY, AIS2100, South Korea). Additionally, energy-dispersive X-ray spectroscopy (EDS) conducted with a TESCAN CO model, MIRA III in Czechia, was utilized to analyse the elemental composition of the sample surfaces. This was done to confirm the successful application of the coatings.

2.5. Fourier transform infrared spectroscopy (FTIR).
FTIR spectroscopy (Thermo Nicolet Avatar, USA) was employed to examine potential structural changes in the bone allografts subsequent to their coating with silver nanoparticles. The tested samples have been mixed with potassium bromide (KBr) salt and prepared as pellets. The samples underwent evaluation within the wavenumber range of 4,000 cm-1 to 500 cm-1, an appropriate span for characterizing bands from both organic and inorganic compounds present in the bone allograft samples. Measurements were conducted with 4 cm-1 steps.

2.6. In vitro antibacterial activity test
The study aimed to evaluate the antibacterial activity of the proposed AgNPs-coated bone allograft. *Staphylococcus aureus* (s. aureus) and streptococcus mutans (s. mutans) were used in this experiment. The bacterial strains
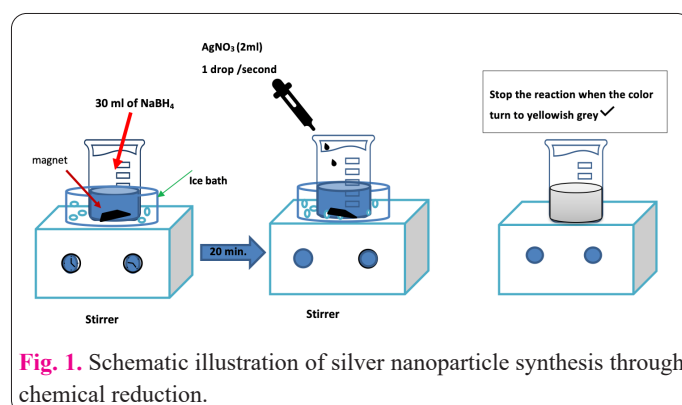
Fig. 1. Schematic illustration of silver nanoparticle synthesis through chemical reduction.

used in this study are commonly identified as pathogens found in bone graft infections [19]. Based on the test results, the optimal concentration of silver nanoparticles has been selected for the subsequent experiment. This minimum concentration, which effectively eradicates bacterial growth on bone allograft samples, will be utilized to assess its biocompatibility.

2.6.1. Minimum inhibitory concentration (MIC) of the synthesized AgNPs

Standard protocol was used for measurement of minimum inhibitory concentration (MIC) as described by Allend et al, [20]. In short, serial two-fold dilutions of AgNPs solution in concentrations ranging from 50 mg/L to 0.1 mg/l with adjusted bacterial inocula (10^8 CFU/ml, 0.5 McFarland's standard) in BHI broth were used. The control groups include inoculated broth and BHI broth alone and incubated for 24 h at 37 °C. The MIC endpoint represents the lowest concentration of silver nanoparticles at which no detectible growth is observed in the tubes. The visual turbidity of the tubes was recorded, confirming the MIC value through spectrophotometric analysis at 630 nm.

2.7. Quantitative and qualitative analysis of AgNPs antibacterial activity

The disk diffusion method was employed to assess the antibacterial effectiveness of the coated bone allograft, following the standardized protocol outlined in [21]. BHI agar plates were swabbed with a fresh culture of pathogenic organisms (10^8 CFU/ml, 0.5 McFarland's standard), then the plates were left to dry for about 2 or 3 min. The agar was aseptically punctured using sterile tips to create 5 mm diameter holes. Subsequently, 50 µL of both coated and uncoated bone allograft samples (dissolved in 1 mL of phosphate buffer saline) were added to the wells (Figure 2). Each treatment was replicated three times and then incubated at 37 °C for 24 hours. Following incubation, the zone of inhibition was measured in millimeters using a measuring ruler, and the means of three measurements were calculated. Prior to experimentation, all samples underwent sterilization via UV irradiation.

In addition to the disk diffusion method, S. aureus and S. mutans were exposed to different coated bone allografts for 24 h. Briefly, the samples (uncoated bone allograft, coated bone allograft, 0.2 % chlorhexidine and blank tube with no sample only inoculum as a reference) were added to each tube containing 1ml of BHI inoculated with (10^8 CFU/ml, 0.5 McFarland's standard) and incubated for 24 h. At the end of the exposure time (24 h), the inhibition of bacterial growth in the external media was investigated by measuring the turbidity of the media [22]. The absorbance was measured at a wavelength of 630 nm using a spectrophotometer (EX800, USA). The silver ion release from the samples was also measured at the end of the exposure time (24 h) using inductively coupled plasma mass spectrometry (ICP-OES 730-ES, Varian).

The biofilm formation on the samples was investigated qualitatively using SEM following the standardized protocol [23]. After exposure time of the samples to the two bacterial species as explained above, the samples were removed from the tube and washed with phosphate buffer saline to eradicate unattached bacteria, and fixed with 2% glutaraldehyde for 2 hours, followed by 1% osmium tetroxide for 15 minutes. Then, the samples were exposed to serial dehydration with a graded series of ethanol solutions (50%, 60%, 70%, 80%, 90%, 99%, and 100% ethanol) for 10 minutes each. Finally, the samples were dried in a critical point dryer and coated with thin layer of gold to make it conductive and visualized by SEM (SERON TECHNOLOGY, AIS2100, South Korea; University of Amir Kabir, Iran).

2.8. In-vitro evaluation of the biocompatibility of the coated bone allograft

This study aimed to explore the biocompatibility and cytotoxicity of the silver nanoparticle-coated bone allograft, assessing whether the application of silver nanoparticles (5 mg/l) on the bone allograft supports the proliferation of the human bone cell line MG63, exhibiting characteristics similar to osteoblast cells. This investigation was conducted quantitatively using the MTT assay and qualitatively via SEM

2.8.1. Preparation and proliferation of MG-63 cells (Human Osteosarcoma cell line)

MG-63 cells (ATCC: C555) were purchased from the National Centre of Genetic Resources in Iran. The cells were cultured in Dulbecco's Modified Eagle Medium (DMEM, CATNO: GIBCO TM 41965039) containing 10% FBS (CATNO: 10082147, GIBCO-USA) and placed in a cell incubator (CO_2 incubator, Binder Company) for the culture to reach the appropriate density.

2.8.2. MTT assay

The cell viability was assessed by using MTT assay. MTT (Cat No.: DMA100) was provided at a concentration of 5 mg/ml in PBS (Cat No.: A-0018). The sterilized samples (uncoated and 5 mg/l AgNPs coated bone allograft) were placed in the culture medium and the cells were cultured on them in a number of about 5×10^3 cells in each well of a 96-well plate in a three-dimensional condition and triplicate and the blank well with no treatment used as a control group. The plate was placed in an incubator for 24 hours and 72 hours.

Following the protocol that was standardized by Mossmann [24], the supernatant was removed and 100 µl of MTT solution with a dilution of 1:10 (MTT initial stock: Culture media) was added to each well. The plates were incubated for 3 to 4 hours at 37°C. The colour of the medium turns purple due to the production of formazan. Later, the

Fig. 2. Disk diffusion method.

Antibacterial AgNPs for bone allograft infection.

Cell. Mol. Biol. 2024, 70(3): 67-77

cell supernatant was removed and 100 μl of dimethyl sulfoxide (DMSO, CATNO: BP231-100) was added to each well to liquefy the produced crystals. Then they were incubated for 15 minutes.

2.8.3. Spectrophotometric data analysis and determination of cell viability

After the addition of DMSO, noticeable changes in cell color occurred: control samples turned purple, indicating cell viability. Lighter well colors corresponded to higher cell death rates. The plate wells were pipetted and in order to read the plate, the samples were removed from the wells after solving the DMSO solvent. Subsequently, the spectrophotometer measured the optical absorbance of the solution at a wavelength of 570 nm. The survival percentage of the cells was calculated using the following formula: (Absorption of treatment sample /absorption of control sample) × 100 = survival percentage of each treatment sample.

2.8.4. Qualitative evaluation with scanning electron microscopy:

For qualitative assessment of cell proliferation, SEM was employed. Briefly, following the seeding of the MG63 cell line on the aforementioned samples, the well plate was incubated for 72 hours. Subsequently, the samples underwent PBS washing to eliminate detached cells and remove residual proteins from the media.

Thereafter the samples were fixed with 2.5% glutaraldehyde in 0.1M Cacodylate buffer for 2 hours. Then, the samples were subjected to sequential dehydration with a graded series of alcohol as mentioned previously. Subsequently, the samples were subjected to drying in a critical point dryer and examined via SEM (SERON TECHNOLOGY, AIS2100, South Korea) at the University of Amir Kabir, Iran. Image analysis was conducted using ImageJ software for quantification, and statistical analysis was performed using Prism software.

2.9. Silver ion release

This study aimed to measure the amount of silver released by the AgNPs-coated bone allograft samples in both in vitro experiments (bacterial and cell culture). Silver concentrations were measured by inductively coupled plasma–optical emission spectrometry (ICP–OES), same protocol followed by Senthil et al, [25]. The calibration formula was measured by using the linear regression algorithm of the ICP–OES instrument software. Three measurements were taken for each sample and the average was determined by the software of the ICP_OES.

2.10. Silver nanoparticles cell penetration

The ability of the synthesized AgNPs to penetrate the eukaryote was also investigated following the same protocol as [26]. To put it succinctly, after seeding MG63 cell line on the bone graft coated AgNPs 5 mg/L stained by Cell Tracker™ CM-DiI Dye (1 μg/mL; Invitrogen, USA) as mentioned above the well plate was incubated for 72 h. For detection AgNPs penetration, the contents of the wells were emptied and the wells were washed with PBS. Then, 100 μL of para-formaldehyde was transferred into each well and incubated for 20 - 30 minutes until the cells were fixed. Afterward, each well was stained with 4', 6-diamidino-2-phenylindole (DAPI, Sigma) at a concentration of

300 nM and snapped with a fluorescence microscope, and the images were analysed. DiI was identified in wavelength Range, of 549 nm and DAPI was detected in wavelength Range 358 nm by fluorescence. The Images were taken by Ziss camera CCD. The images were calculated by ImageJ software and analysed by Prism statically software.

2.11. Statistical Analysis

The data underwent coding and entry using the Graph Pad Prism statistical package (Version 9). Summaries were generated utilizing the mean and standard deviation. Group comparisons were conducted through analysis of variance (ANOVA) alongside the multiple comparisons post hoc test. Statistically significant results were defined as p-values less than 0.05.

3. Results
3.1 X-ray diffraction (XRD)

After synthesizing the silver nanoparticles via chemical reduction, XRD analysis was conducted to investigate the crystalline phase and structure of the AgNPs. The X-ray diffraction pattern of the resultant AgNPs is depicted in Figure **3**. Several Bragg reflection peaks were identified at 2θ values of 38.208°, 44.458°, 64.558°, and 77.558°, corresponding to the (6143.2), (2294.6), (1696.8), and (1765.4) planes of silver NPs. These XRD findings distinctly indicate the crystalline nature of the synthesized Ag nanoparticles.

3.2. FTIR

The FTIR spectra of the AgNPs synthesized by chemical reduction method from 4000 cm^{-1} to 650 cm^{-1}. Figure 4A shows the impact of functional groups around AgNPs by using sodium borohydride ($NaBH_4$). In Figure 4A multiple peaks are observed, signifying the vibrations of chemical bonds between atoms within molecules. The prominent and wide peak in Figure 4A, located at 2982 cm-1, corresponds to the H-C stretching [27]. This peak suggests the presence of capping agents originating from the sodium borohydride.

Capping agents play a critical role in preventing uncontrolled growth of nanoparticles, managing their tendency to clump together, and regulating their solubility in different solvents. The band at 1709 cm^{-1} is associated with the C=O group. While the C=O bond might not directly partake in the reduction process of Ag+ to Ag NPs when utilizing NaBH4, compounds harboring this bond can still wield significant influence over the size, stability, and surface properties of the synthesized nanoparticles
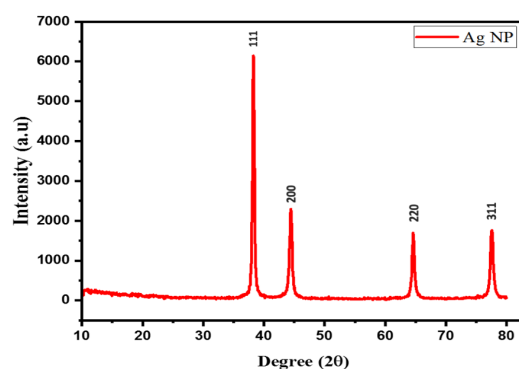
Fig. 3. XRD spectrum of AgNPs.

Antibacterial AgNPs for bone allograft infection.

Cell. Mol. Biol. 2024, 70(3): 67-77

[28]. Here the strong broad band at 1327 cm⁻¹, in Figure 4A belonged to the O-H stretching vibrations of hydroxyl groups. hydroxyl groups may originate from stabilizing agents, solvents, or other compounds utilized during the synthesis procedure [29]. The peak detected at 690 cm-1 in the FTIR spectrum is likely attributed to a compound containing halogen elements.

This compound is thought to form due to the presence of sodium borohydride in the process of synthesizing the Ag NPs [30].

Characterizing the molecular composition of demineralized freeze-dried bone allograft (DFDBA) through FTIR spectroscopy provides valuable insights into its structural components. Figure 4B shows the FT-IR spectra of the DFDBA from 4000 cm⁻¹ to 760 cm⁻¹. The observed band around 3514 cm−1, attributed to the O-H stretching vibrations, appears to be influenced by the DFDBA. This may stem from the presence of hydroxyl groups, especially residual moisture or organic compounds within the bone matrix.

A weak band at around 2800 cm⁻¹ corresponds to the C-H stretching of alkanes. Within biological substrates like demineralized freeze-dried bone allografts (DFDBA), the organic constituents—comprising proteins, lipids, and carbohydrates—display an array of carbon-hydrogen (C-H) bonds within their molecular compositions [31]. The strong band at around 1800 cm⁻¹ Figure 4B is assigned to C=O stretching vibrations, indicative of carbonyl functional groups within the sample. Observing this peak suggests the potential presence of functional groups like ketones, esters, and various organic compounds, commonly found in bone, within the DFDBA matrix. Moreover, the peaks at 1400 cm⁻¹ related to C–C stretching, the presence of peaks in these regions in an FTIR spectrum of a biological or mineral sample might suggest the existence of carbonate ions (CO₃⁻²). In bone materials, carbonate ions can replace some of the phosphate groups in the hydroxyapatite structure, the peaks around 1200 cm−1 indicate the presence of P=O stretching, likely originating from phosphate-containing compounds. This observation potentially signifies the existence of materials like hydroxyapatite, commonly found in bone [32].

The FTIR spectrum illustrating the coating of the bone allograft with silver nanoparticles is presented in Figure 4C. The broad band at 3575 cm⁻¹ is owing to the O-H stretching mode. It can be noticed that this peak is broad in the bone powder due to having more hydroxyl groups. In addition, the peaks at 2900 cm-1 are more likely to belong to the aldehydic C-H stretching mode. The peak at 1800 cm⁻¹ corresponds to the C=O stretching vibration of carboxylic acid groups. The peak that appeared at 1400 cm⁻¹ is due to C–C stretching. The observed peak at 1180 cm-1 is most likely attributed to the P=O stretching.

Additionally, the final absorption band at 876 cm-1 is attributed to the absorption by a compound containing halogen elements. This compound is believed to stem from sodium borohydride in the synthesis process of Ag NPs.

3.3. SEM and EDX analysis
SEM was utilized to validate the presence and distribution of silver nanoparticles on the bone allograft particulate post-physical adsorption coating. Figure 5 demonstrates the absence of silver nanoparticles in the uncoated bone allograft samples.

Based on SEM images, silver nanoparticles were detected on the coated bone allograft, forming aggregates with particle sizes ranging from 95-70 nm. Approximately 70% of the surface area of the bone allograft particulate was covered with silver nanoparticles at a concentration of 50 mg/l. However, the coverage decreased as the concentration of silver nanoparticles decreased, reaching 30% at 10 mg/l and 10% at 5 mg/l, as illustrated in Figure 6.

The EDS analysis confirms the presence of AgNPs on the surface of the bone allograft. The percentage of silver exhibited an upward trend corresponding to the increased concentration of AgNPs used in the coating method, as depicted in Figure 7. A higher percentage of silver was de-
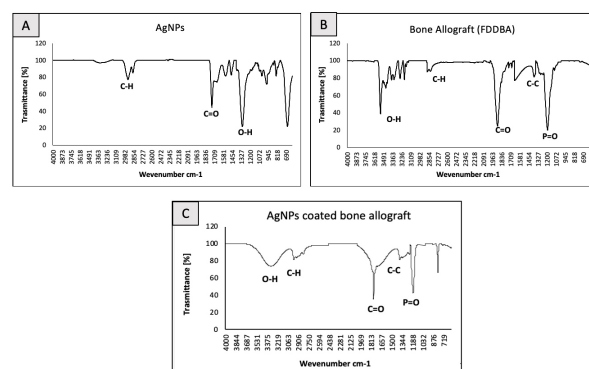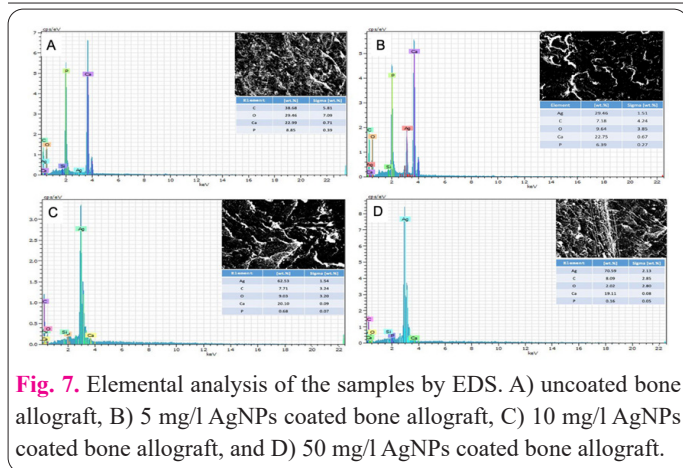

Fig. 4. FTIR spectra of A. AgNPs, B. uncoated bone allograft, C. AgNPs coated bone allograft.
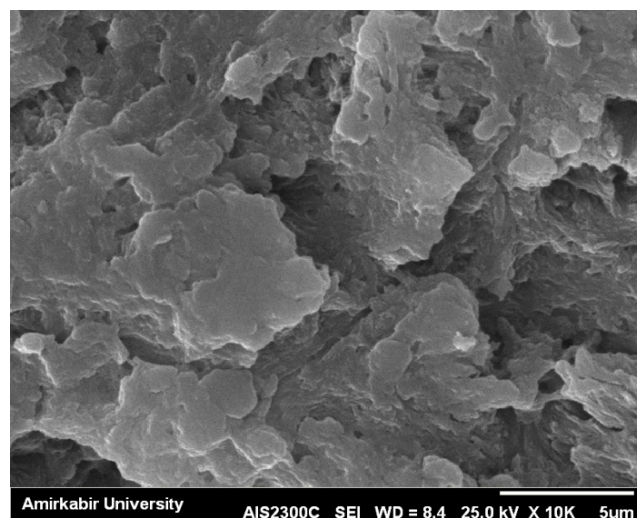
Fig. 5. SEM image of uncoated bone allograft.
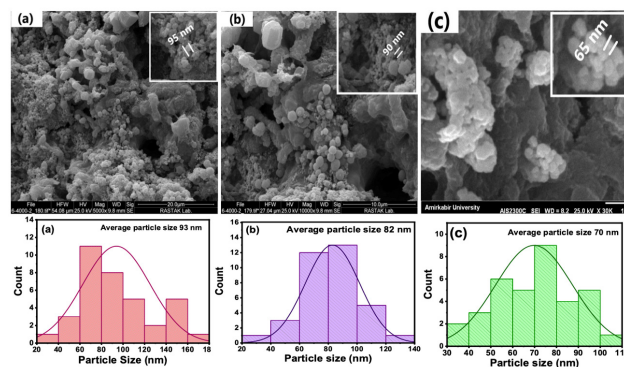
Fig. 6. SEM images of AgNPs coated bone allograft concentration a. 50 mg/l, b. 10 mg/l, c. 5 mg/l AgNPs coated bone allograft.

Antibacterial AgNPs for bone allograft infection.

Cell. Mol. Biol. 2024, 70(3): 67-77

Fig. 7. Elemental analysis of the samples by EDS. A) uncoated bone allograft, B) 5 mg/l AgNPs coated bone allograft, C) 10 mg/l AgNPs coated bone allograft, and D) 50 mg/l AgNPs coated bone allograft.

tected in samples coated with 50 mg/l (70.59 wt.%), while for those coated with 10 mg/l and 5 mg/l, the percentages were 62.53 wt.% and 29.46 wt.%, respectively.

Regarding the wt.% of calcium (Ca), values were 19.11, 20.10, and 22.7 for 50, 10, and 5 mg/l AgNPs-coated bone allograft, respectively, with 22.99 wt.% for the uncoated bone allograft. There was a decrease in the percentage of carbon (C), oxygen (O), and phosphorus (P) with an increase in the concentration of silver used for coating.

In the case of the 50 mg/l silver-coated bone allograft, the wt.% of C, O, and P were 8.09, 2.02, and 0.16, respectively. Conversely, for the 10 mg/l AgNPs-coated bone allograft, these percentages were 7.71, 9.03, and 0.68, respectively. Interestingly, the wt.% of P in the 5 mg/l AgNPs-coated bone allograft showed a minimal difference compared to the uncoated bone allograft, registering 6.39 wt.% for the former and 8.85 wt.% for the latter.

3.4 Antibacterial activity
3.4.1. MIC and turbidity

Both pathogens used in this study exhibited susceptibility to silver nanoparticles, with an MIC of 0.79 mg/l for S. aureus and 0.39 mg/l for S. mutans (data not shown). To assess bacterial growth on both uncoated and AgNPs-coated bone allograft samples, the inhibition of bacterial growth in the culture media was examined after a 24-hour incubation period, measuring turbidity at 630 nm. It was observed that all three concentrations used for bone allograft coating effectively inhibited the growth of both S. aureus and S. mutans, displaying no significant difference from the positive control. However, notable disparities were noted compared to the uncoated bone allograft, as illustrated in Figure 8.

3.4.2. Disk diffusion method

The activity data of AgNPs-coated bone allograft via agar diffusion were depicted in millimetres (mm) and classified based on the presence or absence of inhibition zones. The outcomes revealed that the uncoated bone allograft supported bacterial growth, registering a 0 mm inhibition zone. Conversely, all bone allografts coated with silver nanoparticles successfully inhibited bacterial growth, demonstrating significant differences compared to the uncoated bone allograft (p= 0.000). Additionally, the inhibition zone expanded with higher concentrations of silver nanoparticles.

For S. aureus, the inhibition zones measured 21.33, 13, and 8.33 mm for bone allografts coated with 50, 10, and 5 mg/l AgNPs, respectively (Figure 9A). All tested

groups exhibited significant differences compared to the uncoated bone allograft (p-value < 0.05). Furthermore, the 5 mg/l AgNPs-coated bone allograft showed significant differences compared to the 10 and 50 mg/l AgNPs-coated bone allograft (p < 0.01).

Similarly, AgNPs-coated bone allografts displayed antibacterial activity against S. mutans. The inhibition zones measured 10, 7.66, and 4 mm for bone allografts coated with 50, 10, and 5 mg/l, respectively (Figure 9B). All concentrations exhibited significant differences compared to the uncoated bone allograft, which measured 0.33 mm.

3.4.3. Scanning electron microscopy (SEM):

Examination of the samples through SEM at the end of the incubation period revealed biofilm formation on the surface of the uncoated bone allograft, corroborating the findings from disk diffusion and turbidity tests. Conver-
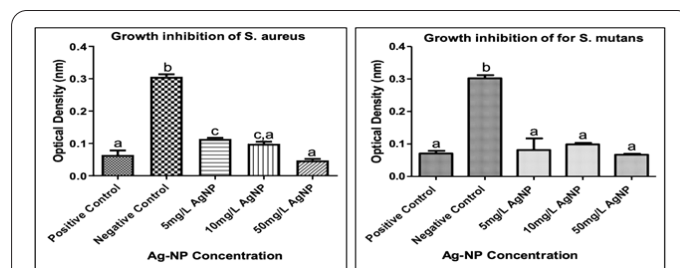

Fig. 8. The inhibition of bacterial growth by measuring turbidity at 630 nm A) S. aureus, and B) S. mutans. (p<0.01).
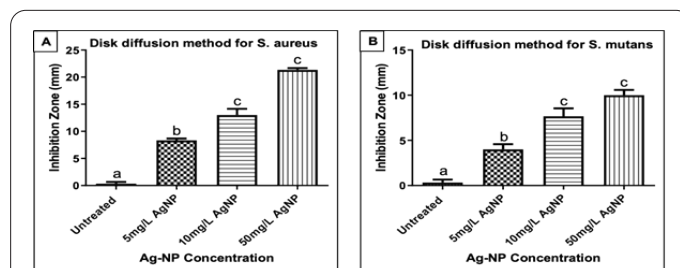
Fig. 9. The graph shows the inhibition zone (mm) of both A) S. aureus and B) S. mutans, (p < 0.05).
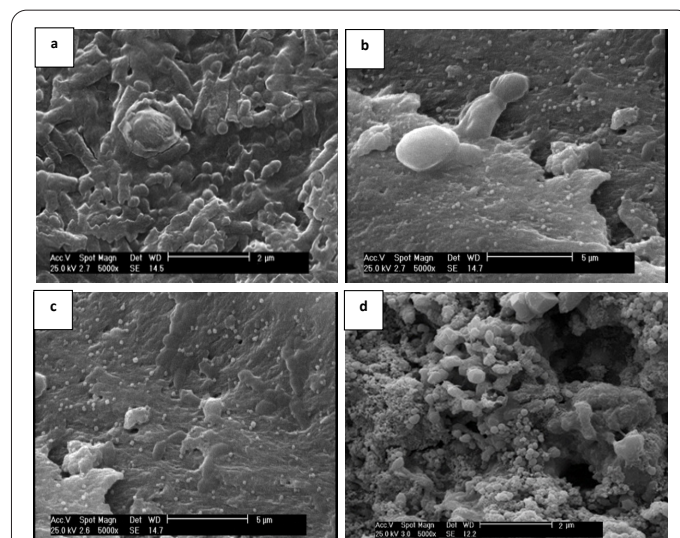
Fig. 10. SEM images of the coated and uncoated bone allograft after 24 h exposure of S. aureus. A. Uncoated bone allograft shows full biofilm coverage, b, c, and d illustrate 5,10,50 mg/l AgNPs coated bone allograft respectively, none of them showed biofilm formation, except for the 5 mg/l AgNPs coated bone allograft show a scarce of bacteria that unable to subdivide.
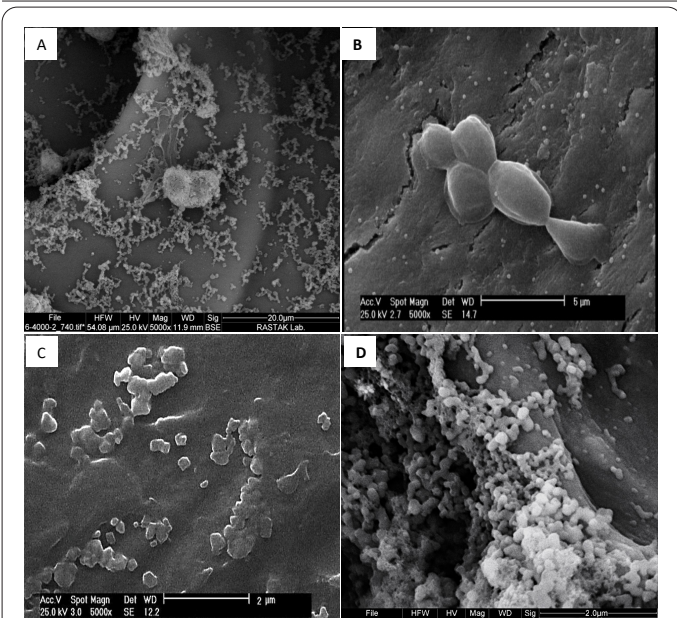
Fig. 11. SEM images of the AgNPs coated and uncoated bone allograft after 24 h exposure of s. Mutans. A. Uncoated bone allograft shows full biofilm coverage, b, c, and d illustrates 5,10,50 mg/l AgNPs coated bone allograft respectively, none of them showed biofilm formation, except for the 5 mg/l AgNPs coated bone allograft shows a bacterial colony that unable to subdivide.

sely, all AgNPs-coated bone allograft samples (5 mg/l, 10 mg/l, and 50 mg/l) displayed a substantial antibiofilm effect, evident from the absence of biofilm formation on the AgNPs-coated bone allograft for both experimental pathogens, S. aureus and S. mutans (Figures 10 and 11). Intriguingly, minimal bacterial colonies were observed.

3.4.4. Total silver concentration

The total concentration of silver released into the external media was assessed using ICP-OES at the culmination of the exposure period for both bacterial tests (Table 1). In the case of the 5 mg/l coated bone allograft, 2.1% of silver was released in the S. aureus test and 2.8% in the S. mutans test. For the 10 mg/l concentration, the release percentages were 1.8% in the S. aureus test and 2.11% in the S. mutans test. Conversely, the release of silver was notably lower for the 50 mg/l AgNPs coated bone allograft, accounting for only 0.57% in the S. aureus test and 0.614% in the S. mutans test. However, no significant differences were detected among the groups.

### 3.5. In vitro biocompatibility investigation

To explore the impact of AgNPs coating on the growth of eukaryotic cells, the MTT test was employed. Illustrated in Figure 12, the AgNPs coating demonstrated no toxic effect on the osteoblast-like MG-63 cell line, evidenced by the absence of significant differences in cell viability percentages across all groups at both 24-hour and 72-hour
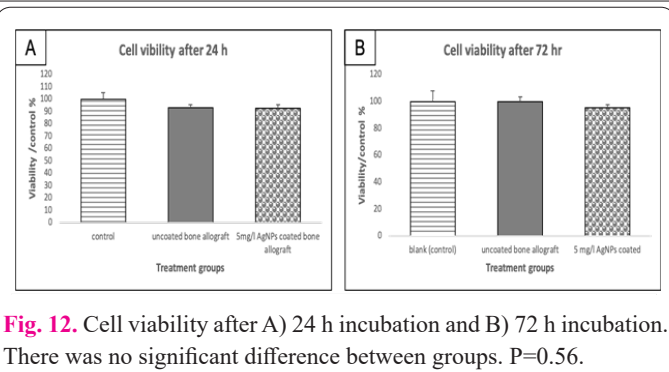
Fig. 12. Cell viability after A) 24 h incubation and B) 72 h incubation. There was no significant difference between groups. P=0.56.
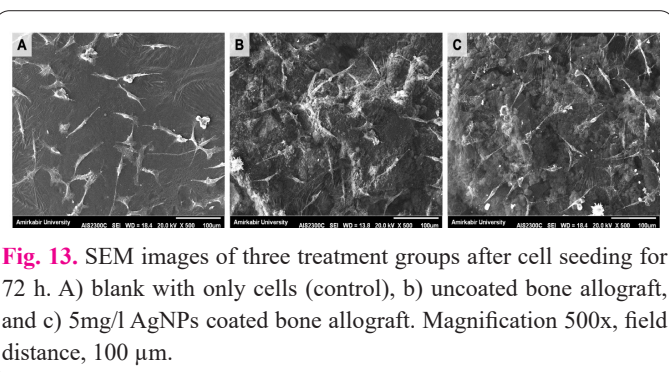
Fig. 13. SEM images of three treatment groups after cell seeding for 72 h. A) blank with only cells (control), b) uncoated bone allograft, and c) 5mg/l AgNPs coated bone allograft. Magnification 500x, field distance, 100 μm.
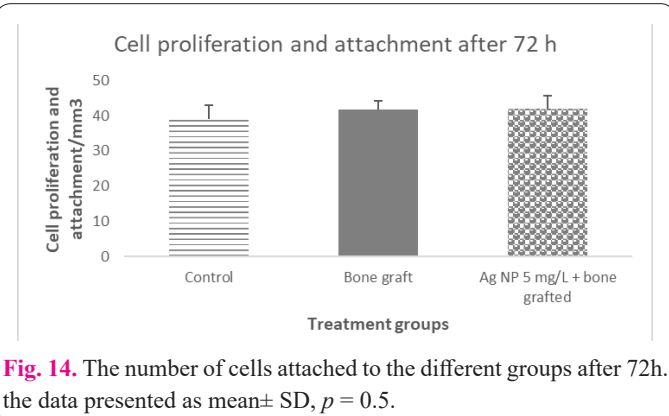
Fig. 14. The number of cells attached to the different groups after 72h. the data presented as mean± SD, *p* = 0.5.

endpoints (p=0.56).

The scanning electron microscopy images exhibited robust growth and attachment of the MG-63 cell line, characterized by the development of pseudopods. All cells displayed elongated spindle shapes, showcasing no discernible differences when compared to the blank and uncoated bone allograft (Figure 13).

The images were quantified using ImageJ software and subjected to analysis using Prism statistical software, presented in Figure 14. The findings indicate that the AgNPs coating did not hinder the cell proliferation on the bone allograft; rather, it promoted cell proliferation.

3.5.1. The total concentration of silver

The total concentrations of silver in the supernatants were examined using ICP-OES after 24 and 72 hours

Table 1. total concentration of silver in external media after 24 h exposure of S. aureus and *S. mutans*.

Samples	Ag NPs release (mg/l) S. aureus	Ag NPs release (mg/l) S. mutans
Uncoated Bone graft	0[#]	0[#]
5 mg/L AgNPs coated bone graft	0.105[*]	0.143[*]
10 mg/L AgNPs coated bone graft	0.180[*]	0.211[*]
50 mg/L AgNPs coated bone graft	0.285[*]	0.307[*]

Antibacterial AgNPs for bone allograft infection.

Cell. Mol. Biol. 2024, 70(3): 67-77

Table 2. The total concentration of silver in the external media after 24 and 72 h.

Treatment groups	Ag NPs (mg/l) After 24 h	Ag NPs (mg/l). After 72 h
Control	0[a]	0[a]
Bone	0[a]	0[a]
5mg/L AgNPs coated bone allograft	0.042[b]	0.071[b]

(Table 2). It was observed that the concentration of silver in the media increased over time. However, no significant difference was noted between the two experimental time points. Yet, a notable distinction was found when compared to the control groups, where no silver was detected in the latter.

3.5.2. AgNPs cell penetration

The capacity of the synthesized AgNPs to penetrate the eukaryotic cells was further examined (Figure 15). Digitized images were captured at a magnification of 100× using a Zeiss Axioplan 2 fluorescent microscope equipped with a DVC system. Subsequent analysis and quantification of the stained cells were conducted using Image J software (version: 1.52h). The result showed that less than 5% of AgNPs were attached to cell membrane and 95% of AgNPs were in cell environment and did not penetrate in the cell cytoplasm.

4. Discussion

Bone graft materials stand as pivotal substances in orthopedic and dental applications for bone regeneration. Various alloplastic or biological materials are commercially available, and their efficacy in bone regeneration is widely acknowledged. Nonetheless, the persisting challenge of infections linked with bone grafting surgery remains a significant concern.

This study was designed to prepare a novel coating for the bone allograft to prevent infection during and after bone grafting procedures. Purchased bone allograft (DFDBA) was coated with chemically synthesized AgNPs in three different concentrations 5,10, and 50 mg/l by physical adsorption. Thereafter, the antibacterial activity of the coated bone allograft was investigated against two pathogens; S. aureus and S. mutans. S. aureus is considered one of the most common pathogens that isolates postoperatively in alveolar bone implants [26]. Furthermore, the cytotoxicity of the coated bone allograft was also investigated using osteoblast-like MG-63 cell line.

The primary discovery is the successful application of the coating method for bone allografts with silver nanoparticles, albeit with some limitations such as silver ion release. This aligns with the findings of a previous study conducted by Xie and colleagues [33]. The release of silver ions was minimal, and their concentrations varied across different media. Particularly, a very low concentration was detected in DMEM (utilized in cell culture tests), which includes fetal bovine serum. This observation suggests that silver likely binds to proteins present in the media [34]. As a result, the free silver was less compared to that detected in the media used for bacterial growth.

The overall trend in the FTIR results indicates the absence of new peaks or substantial alterations in the spectra of the bone allograft after being coated with AgNPs. This suggests a probable physical deposition mechanism rather than a significant chemical interaction between the AgNPs and the bone. Such an observation might imply a
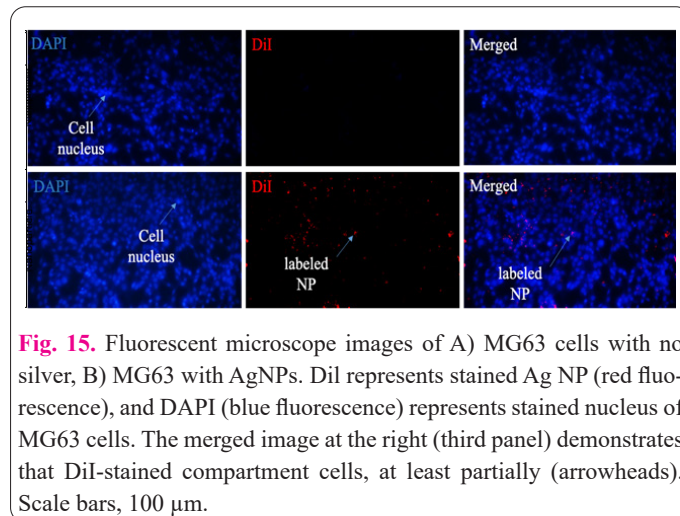
Fig. 15. Fluorescent microscope images of A) MG63 cells with no silver, B) MG63 with AgNPs. DiI represents stained Ag NP (red fluorescence), and DAPI (blue fluorescence) represents stained nucleus of MG63 cells. The merged image at the right (third panel) demonstrates that DiI-stained compartment cells, at least partially (arrowheads). Scale bars, 100 μm.

surface coating process wherein the AgNPs are attached to the bone allograft without inducing significant chemical modifications or generating detectable new chemical entities in the FTIR analysis.

The SEM images demonstrated greater aggregation of the silver nanoparticles in 10 and 50 mg/l concentrations compared to 5 mg/l. Moreover, the nanoparticle size, measured via ImageJ, increased with higher concentrations. This phenomenon is attributed to the tendency of silver nanoparticles to aggregate at higher concentrations in physiological media [35]. The EDS results confirm the success of the physical adsorption method employed in coating the bone allograft with silver nanoparticles, maintaining their attachment even after sample drying. This occurrence may be attributed to the negative charge of hydroxyl radicals from bone (hydroxyapatite) and the positive charge of silver. Consequently, silver nanoparticles could offer an effective mechanism for anchoring [36].

4.1. Antibacterial activity

The coated bone allografts exhibited robust antibacterial activity against the tested pathogens in both suspended and attached bacteria, aligning with findings from prior studies [37, 38]. Multiple theories exist regarding the mechanism of action of silver nanoparticles against bacteria. One suggests the increased surface area of nanoscale silver compared to its metallic particle form allows direct contact with bacteria, enabling penetration of the bacterial cell membrane [15]. Additionally, silver nanoparticles might release silver ions in bacterial culture media, leading to membrane disruption [39]. Silver ions, being positively charged, have a strong affinity to bind with the negatively charged bacterial cell membrane, thereby inhibiting bacterial growth [40]. Consequently, no bacterial growth was observed either in the external media or attached to the surface of the coated bone allograft.

The MIC findings revealed the synthesized AgNPs' potent antibacterial effect, inhibiting S. aureus growth from 0.79 mg/l. This aligns closely with Xia et al.'s study [41], reporting a 1 mg/l MIC for S. aureus. Conversely,

Antibacterial AgNPs for bone allograft infection.

Cell. Mol. Biol. 2024, 70(3): 67-77

Dehkordi et al.'s study found a much higher MIC for S. aureus at 5 mg/l [42], Notably. S. mutans displayed greater sensitivity to silver nanoparticles, with a lower MIC of 0.39 mg/l. However, Subramanian et al [43] and others [44] reported a MIC for S. mutans >1.5 mg/l, indicating variations likely stemming from differences in nanoparticle synthesis methods. The size of the synthesized nanoparticles significantly influences their antibacterial activity, as indicated by [45] highlighting that smaller particle sizes correlate with enhanced antibacterial effects.

4.2. The biocompatibility of the AgNPs

The coated bone allograft demonstrated no cytotoxic effects on the tested eukaryotic cells. Both the cell viability (MTT) assay and SEM imaging indicated no reduction in cell viability or alterations in cell attachment to the bone graft material. The concentration of silver nanoparticles utilized was effective in bacterial eradication without inducing toxicity in the MG-63 cell line. Consistent with other studies [46], it is established that low concentrations of silver nanoparticles, such as <5 mg/l, do not impede cell proliferation compared to the control group [47].

The fluorescent microscopy assessment of AgNPs' penetration into MG-63 cells revealed that the nanoparticles were unable to breach the cell membrane. Instead, only approximately 5% of the AgNPs adhered to the outer surface of the cells without internalization. This observation could be attributed to the larger size of the AgNPs relative to the permeability of the MG-63 cell line (figure 13).

5. Conclusion

Numerous studies have demonstrated the antibacterial efficacy of silver nanoparticles (AgNPs). Nevertheless, concerns persist regarding the potential cytotoxicity of AgNPs on eukaryotic cells, prompting ongoing investigations. In this study, an approved bone allograft was coated with AgNPs at a concentration that fulfills essential criteria for grafting materials: exhibiting potent antibacterial activity without hindering bone cell proliferation. However, this study presents limitations and raises further inquiries. For instance, assessing the durability of the coating material, elucidating the precise mechanism underlying the antimicrobial action of AgNPs, and evaluating the cytotoxic effects of higher concentrations of silver nanoparticles are essential areas warranting additional exploration.

Conflict of interests
The author has no conflicts with any step of the article preparation.

Consent for publications
The author read and approved the final manuscript for publication.

Ethics approval and consent to participate
No human or animals were used in the present research.

Informed consent
The authors declare not used any patients in this research.

Availability of data and material
The data that support the findings of this study are available from the corresponding author upon reasonable request.

Authors' contributions
SD; designed the study work, performed the experiments, analysed the data, wrote the manuscript. OO; darfted and edited the manuscript.

References

1. Hitti RA (2011) Guided Bone Regeneration in the Oral Cavity: A Review. Open Pathol J 5 (1): 33–45. doi: 10.2174/1874375701105010033.

2. Van Der Weijden F, Dell'Acqua F, Slot DE (2009) Alveolar bone dimensional changes of post-extraction sockets in humans: A systematic review. J Clin Periodontol 36 (12): 1048–1058. doi: 10.1111/j.1600-051X.2009.01482.x.

3. Fesseha H, Fesseha Y (2020) Bone Grafting, Its Principle and Application: A Review. Osteol Rheumatol Open J 1 (1): 43–50. doi: 10.17140/ORHOJ-1-113.

4. Schmidt AH (2021) Autologous bone graft: Is it still the gold standard? Injury 52 (5): S18–S22. doi: 10.1016/j.injury.2021.01.043.

5. Manop K, Rui Z, Kiatanant B, Ratchapin LS, Suphachai S, Verasak P, et al (2021) Physicochemical and osteogenic properties of chairside processed tooth derived bone substitute and bone graft materials. Dent Mater J 40 (1): 173–183. doi: 10.4012/dmj.2019-341.

6. Bohner M (2010) Resorbable biomaterials as bone graft substitutes. Mater Today 13 (1–2): 24–30. doi: 10.1016/S1369-7021(10)70014-6.

7. Kim Y-K, Lee J, Um I-W, Kim K-W, Murata M, Akazawa T, et al (2013) Tooth-derived bone graft material. J Korean Assoc Oral Maxillofac Surg 39 (3): 103. doi: 10.5125/jkaoms.2013.39.3.103.

8. Park S-M, Um I-W, Kim Y-K, Kim K-W (2012) Clinical application of auto-tooth bone graft material. J Korean Assoc Oral Maxillofac Surg 38 (1): 2. doi: 10.5125/jkaoms.2012.38.1.2.

9. Delloye C, Cornu O, Druez V, Barbier O (2007) Bone allografts. What they can offer and what they cannot. J Bone Jt Surg - Ser B 89 (5): 574–579. doi: 10.1302/0301-620X.89B5.19039.

10. Ketonis C, Barr S, Adams CS, Shapiro IM, Parvizi J, Hickok NJ (2011) Vancomycin bonded to bone grafts prevents bacterial colonization. Antimicrob Agents Chemother 55 (2): 487–494. doi: 10.1128/AAC.00741-10.

11. Basma H, Misch C (2021) Extraction Socket Grafting and Ridge Augmentation Failures Associated with Clindamycin Antibiotic Therapy: A Retrospective Study. Int J Oral Maxillofac Implants 36 (1): 122–125. doi: 10.11607/jomi.8461.

12. Giannoudis P V, Dinopoulos H, Tsiridis E (2005) Bone substitutes: an update. Injury 36 (3): S20–S27.

13. Coelho CC, Araújo R, Quadros PA, Sousa SR, Monteiro FJ (2019) Antibacterial bone substitute of hydroxyapatite and magnesium oxide to prevent dental and orthopaedic infections. Mater Sci Eng C 97 529–538. doi: 10.1016/j.msec.2018.12.059.

14. Allaker RP (2010) Critical review in oral biology & medicine: The use of nanoparticles to control oral biofilm formation. J Dent Res 89 (11): 1175–1186. doi: 10.1177/0022034510377794.

15. Mathur P, Jha S, Ramteke S, Jain NK (2018) Pharmaceutical aspects of silver nanoparticles. Artif Cells, Nanomedicine Biotechnol 46 (sup1): 115–126. doi: 10.1080/21691401.2017.1414825.

16. Abd-Elkawi M, Sharshar A, Misk T, Elgohary I, Gadallah S (2023) Effect of calcium carbonate nanoparticles, silver nanoparticles and advanced platelet-rich fibrin for enhancing bone healing in a rabbit model. Sci Rep 13 (1): 15232. doi: 10.1038/s41598-023-42292-x.

Antibacterial AgNPs for bone allograft infection.

Cell. Mol. Biol. 2024, 70(3): 67-77

17. Van Dong P, Ha CH, Binh LT, Kasbohm J (2012) Chemical synthesis and antibacterial activity of novel-shaped silver nanoparticles. Int Nano Lett 2 (1): 1–9. doi: 10.1186/2228-5326-2-9.

18. González-Sánchez MI, Perni S, Tommasi G, Morris NG, Hawkins K, López-Cabarcos E, et al (2015) Silver nanoparticle based antibacterial methacrylate hydrogels potential for bone graft applications. Mater Sci Eng C 50 332–340. doi: 10.1016/j.msec.2015.02.002.

19. Nisyrios T, Karygianni L, Fretwurst T, Nelson K, Hellwig E, Schmelzeisen R, et al (2020) High potential of bacterial adhesion on block bone graft materials. Materials (Basel) 13 (9): 2102. doi: 10.3390/ma13092102.

20. Allend SO, Garcia MO, da Cunha KF, de Albernaz DTF, da Silva ME, Ishikame RY, et al (2022) Biogenic silver nanoparticle (Bio-AgNP) has an antibacterial effect against carbapenem-resistant Acinetobacter baumannii with synergism and additivity when combined with polymyxin B. J Appl Microbiol 132 (2): 1036–1047. doi: 10.1111/jam.15297.

21. Suresh S, Karthikeyan S, Saravanan P, Jayamoorthy K (2016) Comparison of antibacterial and antifungal activities of 5-amino-2-mercaptobenzimidazole and functionalized NiO nanoparticles. Karbala Int J Mod Sci 2 (3): 188–195. doi: 10.1016/j.kijoms.2016.05.001.

22. Hadi SD (2014) The Antibacterial Properties and Biocompatibility of Silver and Hydroxyapatite Nanoparticles Coating on Dental Implants. (May): 132.

23. Zhang H, Komasa S, Mashimo C, Sekino T, Okazaki J (2017) Effect of ultraviolet treatment on bacterial attachment and osteogenic activity to alkali-treated titanium with nanonetwork structures. Int J Nanomedicine 12 4633–4646. doi: 10.2147/IJN.S136273.

24. Mosmann T (1983) Rapid colorimetric assay for cellular growth and survival: Application to proliferation and cytotoxicity assays. J Immunol Methods 65 (1–2): 55–63. doi: 10.1016/0022-1759(83)90303-4.

25. Schlich K, Klawonn T, Terytze K, Hund-Rinke K (2013) Effects of silver nanoparticles and silver nitrate in the earthworm reproduction test. Environ Toxicol Chem 32 (1): 181–188. doi: 10.1002/etc.2030.

26. Nie B, Long T, Ao H, Zhou J, Tang T, Yuea B (2017) Covalent immobilization of enoxacin onto titanium implant surfaces for inhibiting multiple bacterial species infection and in vivo methicillinresistant staphylococcus aureus infection prophylaxis. Antimicrob Agents Chemother 61 (1): 10–1128. doi: 10.1128/AAC.01766-16.

27. Miranda A, Akpobolokemi T, Chung E, Ren G, Raimi-Abraham BT (2022) pH Alteration in Plant-Mediated Green Synthesis and Its Resultant Impact on Antimicrobial Properties of Silver Nanoparticles (AgNPs). 11 (11): 1592. doi: 10.3390/antibiotics11111592.

28. Cui L, Chen P, Chen S, Yuan Z, Yu C, Ren B, et al (2013) In situ study of the antibacterial activity and mechanism of action of silver nanoparticles by surface-enhanced raman spectroscopy. Anal Chem 85 (11): 5436–5443. doi: 10.1021/ac400245j.

29. Senthil B, Devasena T, Prakash B, Rajasekar A (2017) Non-cytotoxic effect of green synthesized silver nanoparticles and its antibacterial activity. J Photochem Photobiol B Biol 177 1–7. doi: 10.1016/j.jphotobiol.2017.10.010.

30. Mondal MS, Paul A, Rhaman M (2023) Recycling of silver nanoparticles from electronic waste via green synthesis and application of AgNPs-chitosan based nanocomposite on textile material. Sci Rep 13 (1): 13798. doi: 10.1038/s41598-023-40668-7.

31. Wang QS, Zhu XN, Jiang HL, Wang GF, Cui YL (2015) Protective effects of alginate–chitosan microspheres loaded with alkaloids from Coptis chinensis Franch. and Evodia rutaecarpa (Juss.) Benth. (Zuojin Pill) against ethanol-induced acute gastric mucosal injury in rats. Drug Des Devel Ther 9 6151–6165. doi: 10.2147/DDDT.S96056.

32. Dalavi PA, Prabhu A, Shastry RP, Venkatesan J (2020) Microspheres containing biosynthesized silver nanoparticles with alginate-nano hydroxyapatite for biomedical applications. J Biomater Sci Polym Ed 31 (16): 2025–2043. doi: 10.1080/09205063.2020.1793464.

33. Xie CM, Lu X, Wang KF, Meng FZ, Jiang O, Zhang HP, et al (2014) Silver nanoparticles and growth factors incorporated hydroxyapatite coatings on metallic implant surfaces for enhancement of osteoinductivity and antibacterial properties. ACS Appl Mater Interfaces 6 (11): 8580–8589. doi: 10.1021/am501428e.

34. Hansen U, Thünemann AF (2015) Characterization of Silver Nanoparticles in Cell Culture Medium Containing Fetal Bovine Serum. 31 (24): 6842–6852. doi: 10.1021/acs.langmuir.5b00687.

35. Prathna TC, Chandrasekaran N, Mukherjee A (2011) Studies on aggregation behaviour of silver nanoparticles in aqueous matrices: Effect of surface functionalization and matrix composition. Colloids Surfaces A Physicochem Eng Asp 390 (1–3): 216–224. doi: 10.1016/j.colsurfa.2011.09.047.

36. Buckley JJ, Lee AF, Olivi L, Wilson K (2010) Hydroxyapatite supported antibacterial Ag 3 PO 4 nanoparticles. J Mater Chem 20 (37): 8056–8063.

37. Kung JC, Wang WH, Lee CL, Hsieh HC, Shih CJ (2020) Antibacterial activity of silver nanoparticles (Agnp) confined to mesostructured, silica-based calcium phosphate against methicillin-resistant staphylococcus aureus (mrsa). 10 (7): 1–14. doi: 10.3390/nano10071264.

38. Gonçalves GA, Ribeiro VST, Dantas LR, de Andrade AP, Suss PH, Witt MA, et al (2023) Antimicrobial Activity of Bovine Bone Scaffolds Impregnated with Silver Nanoparticles on New Delhi Metallo-β-Lactamase-Producing Gram-Negative Bacilli Biofilms. 3 (4): 584–595. doi: 10.3390/compounds3040042.

39. Prabhu S, Poulose EK (2012) Silver nanoparticles: mechanism of antimicrobial action, synthesis, medical applications, and toxicity effects. Int nano Lett 2 (1): 32.

40. Dibrov P, Dzioba J, Gosink KK, Häse CC (2002) Chemiosmotic mechanism of antimicrobial activity of Ag+ in Vibrio cholerae. Antimicrob Agents Chemother 46 (8): 2668–2670. doi: 10.1128/AAC.46.8.2668-2670.2002.

41. Xia QH, Ma YJ, Wang JW (2016) Biosynthesis of silver nanoparticles using Taxus yunnanensis callus and their antibacterial activity and cytotoxicity in human cancer cells. 6 (9): 160. doi: 10.3390/nano6090160.

42. Dehkordi SH, Hosseinpour F, Kahrizangi AE (2011) An in vitro evaluation of antibacterial effect of silver nanoparticles on Staphylococcus aureus isolated from bovine subclinical mastitis. African J Biotechnol 10 (52): 10795–10797. doi: 10.5897/ajb11.1499.

43. Subramanian P, Ravichandran A, Manoharan V, Muthukaruppan R, Somasundaram S, Pandi B, et al (2019) Synthesis of Oldenlandia umbellata stabilized silver nanoparticles and their antioxidant effect, antibacterial activity, and bio-compatibility using human lung fibroblast cell line WI-38. Process Biochem 86 196–204. doi: 10.1016/j.procbio.2019.08.002.

44. Hernández-Sierra JF, Ruiz F, Cruz Pena DC, Martínez-Gutiérrez F, Martínez AE, de Jesús Pozos Guillén A, et al (2008) The antimicrobial sensitivity of Streptococcus mutans to nanoparticles of silver, zinc oxide, and gold. Nanomedicine Nanotechnology, Biol Med 4 (3): 237–240. doi: 10.1016/j.nano.2008.04.005.

45. Espinosa-Cristóbal LF, Martínez-Castañón GA, Martínez-Martínez RE, Loyola-Rodríguez JP, N. Patiño-Marín, Reyes-Macías JF, et al (2009) Antibacterial effect of silver nanoparticles against Streptococcus mutans. Mater Lett 63 (29): 2603–2606. doi:

Antibacterial AgNPs for bone allograft infection.

Cell. Mol. Biol. 2024, 70(3): 67-77

10.1016/j.matlet.2009.09.018.

46. Pauksch L, Hartmann S, Rohnke M, Szalay G, Alt V, Schnettler R, et al(2014) Biocompatibility of silver nanoparticles and silver ions in primary human mesenchymal stem cells and osteoblasts. Acta Biomater 10 (1): 439–449. doi: 10.1016/j.actbio.2013.09.037.

47. Xie H, Wang P, Wu J (2019) Effect of exposure of osteoblast-like cells to low-dose silver nanoparticles: uptake, retention and osteogenic activity. Artif Cells, Nanomedicine Biotechnol 47 (1): 260–267. doi: 10.1080/21691401.2018.1552594.